MULTI-PHYSICS MOLECULAR-DYNAMICS-FEM FOR THE VIRTUAL DESIGN OF NANO-STRUCTURES AND DEVICES TOWARDS PROPERTY SPECIFICATIONS ACROSS SCALES

André A.R. Wilmes*, Silvestre T. Pinho

Department of Aeronautics, Imperial College London, South Kensington Campus,
London SW7 2AZ, United Kingdom. Email: andre.wilmes07@imperial.ac.uk,
silvestre.pinho@imperial.ac.uk . Web Page: www.imperial.ac.uk/people/silvestre.pinho

Keywords: MDFEM, multi-scale, multi-physics, graphene, toughness, rotational boundary conditions

Abstract

The rise of 2D materials has accelerated progress in nano-synthesis, and while single atom devices are manufactured, scalable techniques (e.g. CVD) have brought materials with tuneable nano-structures to the structural engineering scales; thereby creating design spaces for tailoring material properties across previously unattainable scales. Therefore, modelling communities must follow the integration of the physics, chemistry and synthesis fields, and accelerate their efforts towards an integrated virtual engineering design environment, so that future material innovations remain economically feasible.

This work presents a mathematically rigorous and novel-featured molecular dynamics finite element method (MDFEM), which implements any MD force field (e.g. reactive, charge-dipole) within an FEM solver. Novel boundary conditions (OBC) are presented for accurately capturing bending deformations in structures, discrete or continuum, which modularly achieve property homogenisation across scales and physical representations; thereby enabling MDFEM multi-scale and -physics integration. Numerical implementations of the MDFEM and OBC are achieved within minutes using a network-theory-inspired code generator with novel motif-detection meshing algorithms for a priori unknown element topologies.

Thus, this work presents an integrated engineering design environment, which is applicable from the smallest scales, for resolving a nano-device's electro-mechanical behaviour, to the larger scales, for virtually testing nano-structures for properties of engineering interest such as graphenes fracture toughness.

1. Introduction

Recently, spatial scales-based boundaries between disciplines such as physics, chemistry and engineering have largely eroded. In particular with 2D materials, physicists and chemists have bridged the separation between the physically discrete nano/micro-scales (i.e. Å–μm), and the traditionally continuum-described micro/macro-scales (i.e. μm–m). High-fidelity technologies (e.g. CVD [1], nanoimprint litography [2, 3]), now permit to pattern 3D nano-features of 10–30 nm over meter-scale 2D crystal domains. Thus, the engineering design possibilities and the scope for multi-physics functionalities and synergistic gains, which open in these new design spaces, are nearly limitless for the virtual optimisation and tailoring of device designs and material bulk properties towards target specifications.

It follows that the fields of material modelling must follow the above integration across scales and discipline boundaries in order to achieve a truly ***integrated virtual engineering design and simulation environment***, which readily and seamlessly integrates across all scales and physics. This objective is of pivotal technological significance and financial impact, as within the near endless design spaces, the development of novel material classes and devices with synergistic property effects, at economically feasible costs, inherently requires virtual engineering designing, guidance and optimisation.

Excerpt from ISBN 978-3-00-053387-7

This paper pursues this integration by (i) presenting a MDFEM [4], exactly embedding the equilibrium equations of any multi-physics MD force field within the more versatile FEM, see § 2; (ii) presenting novel Objective Boundary Conditions (OBC) [5], which exactly represent rotational symmetries in structures with local and non-local physics, and homogenise their multi-physics response for any chosen continuum idealisation, see § 3; and (iii) outlines a code generator which achieves numerical implementations of the MDFEM and OBC within minutes using a network-theory-inspired code generator with novel motif-detection meshing algorithms for admitting a priori unknown element topologies, see § 4.

2. Molecular Dynamics Finite Element Method

Hamilton's Principle is a formal and natural approach to describe dynamic equilibrium in a discrete or discretised multi-physics domain, and can lead to Lagrange's equation for any system described in n generalised displacements, denoted by $\mathbf{q}$, where the generalised external forces are denoted by $\mathfrak{f}$, the multi-physics conservative generalised potential energy by V and, the generalised kinetic co-energy by T^*. At the MD level of theory, the set of translational displacements, $\mathbf{u}$, partial electric charges, $\mathbf{q}$, and electric dipoles, $\mathbf{p}$, of all atoms constitutes a comprehensive and natural choice of $\mathbf{q}$ for a discrete particle system, as shown in Fig. 1(a). Noting that, for a multi-physics domain, the kinetic co-energy may generally be non-quadratic and potentially positive semi-definite, it follows that Lagrange's equation becomes [4]:

$$\mathbf{M}(\dot{\mathbf{q}})\,\ddot{\mathbf{q}} + \nabla_{\mathbf{q}}(V(\mathbf{q})) = \mathbf{M}(\dot{\mathbf{q}})\,\ddot{\mathbf{q}} + \left(\mathbf{J}_{\mathbf{q}}^{V}\right)^{\mathrm{T}} = \mathfrak{f}\,, \tag{1}$$

where $\nabla_{\mathbf{q}}(V(\mathbf{q}))$ is the transpose of the generalised potential's Jacobian relative to the system's displacements. The generalised mass matrix, $\mathbf{M}(\dot{\mathbf{q}})$, is unique, symmetric, potentially non-linear, either positive definite and non-singular or, positive semi-definite and singular. Eq. (1) suggest an analogy with the FEM and can be solved within FEM schemes, given the $\mathbf{M}(\dot{\mathbf{q}})$, $\mathbf{J}_{\mathbf{q}}^{V}$ and $\mathbf{H}_{\mathbf{q}}^{V}$ [4].

A system's MD potential energy generally consists of sub-potentials, V_S (e.g. bond stretch, bending), each of which can be sub-divided into n_p^S repeating partitions, namely:

$$V(\mathbf{c}) = \sum_{\mathbb{S}} V_S(\mathbf{c}_S) = \sum_{\mathbb{S}} \sum_{i=1}^{n_p^S} V_S^i\left(\mathbf{c}_S^i\left(\mathfrak{x}_S^i, \mathbf{q}_S^i\right)\right), \tag{2}$$

where $\mathbf{c}$ represents the potential's characteristic variables (e.g. bond lengths). Classical force fields include sub-potentials for mechanical deformation modes (e.g. stretching), while charge-dipole potentials cause electro-mechanical couplings. Hence, each partition may takes the role of an "element" within the FEM terminology, with an element topology for each sub-potential partitioning pattern. These are superposed in layers during meshing, which outlines a fundamental difference between the MDFEM [4] and the classical FEM. The element topology naturally follow the respective characteristic variable-defining sketches, see Fig. 1(b). Using the FEM-typical element assembly approach, only the local Jacobian and Hessian within each element are required for solving the global equilibrium (i.e. Eq. (1)). These tensors are obtained indirectly, using chain derivatives, which maintains an uncoupling of the chemical force field constitutive information from the spacial geometrical behaviour of the characteristic variables [4].

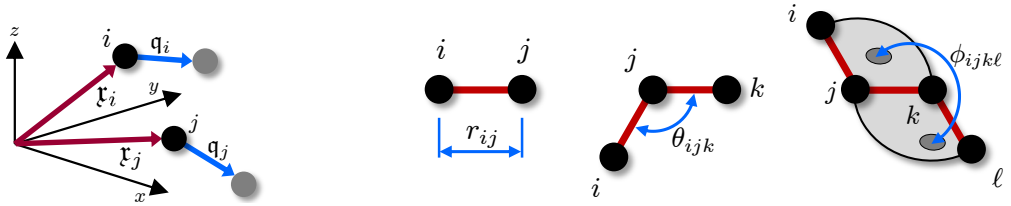

(a) Generalised displacements (b) MD force field characteristic variables for sub-potentials

Figure 1. Generalised displacements for atoms i and j and selected MD characteristic variables.

Excerpt from ISBN 978-3-00-053387-7

3. Objective Boundary Conditions & Property Homogenisation

Periodic Boundary Conditions (PBC) cannot capture rotational/orthogonal symmetries, which occur with low-dimensional compounds (e.g. nanotubes), both in the base and loaded state (e.g. bending/torsion), as exemplified by the discrete/discretised domain in Fig. 2 where material points are depicted by ● , matching UC boundaries by |, while local and non-local energy interactions are denoted by | and ¦.

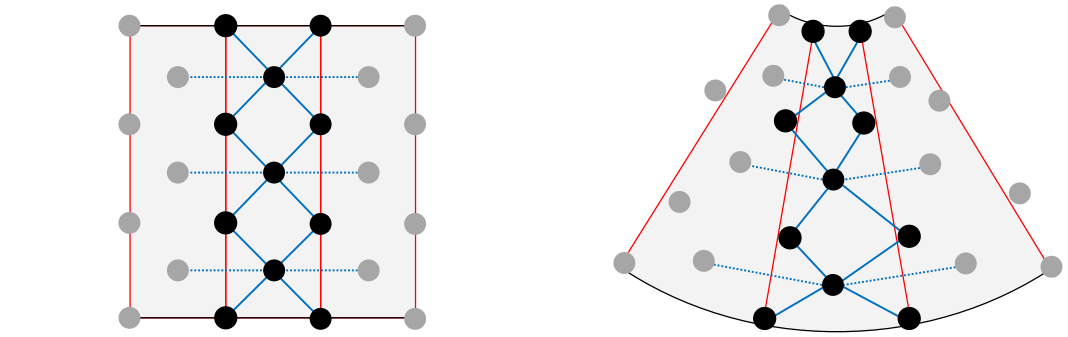

(a) Discrete UC with local & non-local physics (b) A deformed UC with orthogonal transformations

Figure 2. Objective structure UC with local & non-local physics during bending.

Hereafter, the Objective Boundary Condition formulation [5] is presented, which: (i) can account for orthogonal transformations with the resulting physics-based geometrical non-linearities between matching Unit Cell (UC); (ii) is applicable to both discrete- and continuum-physics governed domains, with both local and non-local interactions (i.e. non-local physics, where material points from several UC away interact, require cumulative rotations); (iii) inherently and robustly bridges the gap between scales, discrete-to-continuum as well as continuum-to-continuum through implicit property homogenisation; (iv) while posing no risk for artificially suppressing or altering the UC mirco-field.

The OBC Unit Cell is modularly constituted of a: (i) *Physical Unit* (PU), which is a repeating, continuous or discrete, physical subdomain of an infinite structure up to orthogonal transformations, where each material point i has generalised positions, $\mathfrak{r}_i$; (ii) *Simulation Domain* (SD), which is a purely geometrical, continuous and deformable reference object (e.g. 1D curves, 2D surfaces), with a parametrically defined ground state $\mathbf{x}_{\text{sd}}(\mathbf{s}_{\text{sd}})$; (iii) *Tessellation & Periodicity Dimensionality* (PD), which denotes the number of chosen tessellation directions of a continuous, monohedral and congruent objective tessellation for the chosen SD; and a (iv) *Kinematic Behaviour* (KB), which associates with the SD a continuous distribution of generalised properties, governed by a parametric vector function, $\boldsymbol{\Upsilon}^{\mathbf{u}}_{\text{sd}}$, which is dependent on $n_{\mathfrak{e}}$ arbitrary free *kinematic parameters* $\mathfrak{e}$ (i.e. the deformed SD is given by $\mathbf{r}_{\text{sd}}(\mathbf{x}_{\text{sd}}, \mathfrak{e}) = \mathbf{x}_{\text{sd}} + \boldsymbol{\Upsilon}^{\mathbf{u}}_{\text{sd}}(\mathbf{x}_{\text{sd}}, \mathfrak{e})$.)

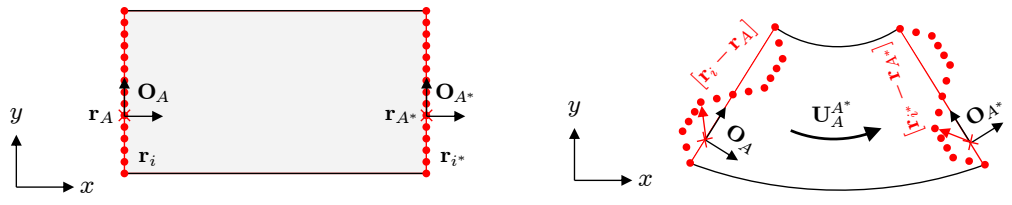

(a) Corresponding material boundary points (b) Local boundary profiles must coincide

Figure 3. 1st order OBC enforces local boundary equivalence at corresponding boundaries.

The 1st order variant of the OBC [5] applies to UC with strictly local physics and with overlapping material points at the UC boundaries, depicted by ● in Fig. 3(a). This OBC variant enforces the PU boundary deformation profile, as locally observed from two corresponding points A and A^* on the SD object, to be identical up to and including orthogonal transformations, see Fig. 3(b). This is stated as:

Excerpt from ISBN 978-3-00-053387-7

$$\mathbf{r}_{i^*} - \mathbf{r}_{A^*}(\boldsymbol{\epsilon}) = \mathbf{U}_A^{A*}(\boldsymbol{\epsilon})\,[\mathbf{r}_i - \mathbf{r}_A(\boldsymbol{\epsilon})]\ , \tag{3}$$

where i and i^* denote corresponding material points, and the unitary matrix, $\mathbf{U}_A^{A*} = \mathbf{U}_A^{A*}(\boldsymbol{\epsilon}) = \mathbf{O}_A\,(\mathbf{O}_{A*})^{-1}$, describes the rotation between the SD spacial orientations at the points A and A^*, denoted by $\mathbf{O}_A$ and $\mathbf{O}_{A^*}$, which are readily obtained from the spatial gradient of the KB parametric function $\mathbf{r}_{\mathrm{sd}}(\mathbf{x}_{\mathrm{sd}}, \boldsymbol{\epsilon})$. For multi-physics domains, a generalised form of Eq. (3) holds, which is enforced by any constraint method.

A 2nd order variant of the OBC [5] applies to UC with non-local physics, where the required non-local material points outside the UC are mapped first using the SD points A and A^*, which allows the potential energy of the system to be expressed in terms of the local material points $\mathbf{r}_i$ and the kinetic parameters $\boldsymbol{\epsilon}$ only. The element topologies for representing such non-local energies do not physically correspond to their interaction, but are a set of core UC materials points required and an external node with $\boldsymbol{\epsilon}$, see Fig. 4.

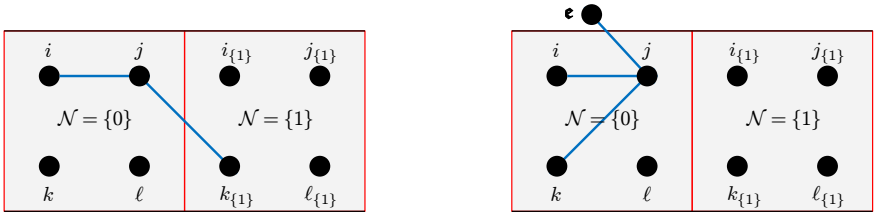

(a) Non-local 3-node energy interaction (b) Non-local topology for a 3-node interaction

Figure 4. Non-local element topologies do not physically match the interaction they represent.

Both the 1st and 2nd order OBC may be applied to systems described by Eq. (1), where the global solution minimises not only the PU generalised coordinates, $\mathbf{q}$, but the SD *kinematic parameters*, $\boldsymbol{\epsilon}$, as well. If the KB parametric function, $\mathbf{r}_{\mathrm{sd}}(\mathbf{x}_{\mathrm{sd}}, \boldsymbol{\epsilon})$, respects the kinematic assumptions of a structural theory (e.g. plate theory), and $\boldsymbol{\epsilon}$ are chosen to coincide with the theory's strain components, then the homogenised stress state and thereby the constitutive relations are implicitly obtained during the energy minimisation as the generalised forces corresponding to $\boldsymbol{\epsilon}$. The modular composition of the OBC UC allows for the homogenisation of a PU as objects of varying dimensionality, form and kinematic behaviour, see Fig. 5.

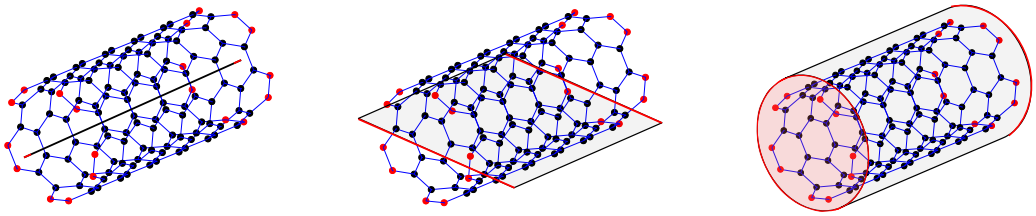

(a) CNT homogenised as a 1D wire (b) CNT homogenised as a 2D plate (c) CNT homogenised as a 3D tube

Figure 5. Properties of physical units may be homogenised for different structural idealisations.

4. MDFEM-OBC code generator & network-based element meshing

The MDFEM and OBC formulations were implemented symbolically in MATLAB, where readily extendible libraries contain MD force fields, characteristic variable definitions and OBC kinematic behaviour functions. All MDFEM and OBC tensors are symbolically derived and analytically optimised. The resultant algebraic expression are further optimised numerically, and exported in a desired language form (e.g. FORTRAN-90/95) suitable for a chosen implicit and explicit FEM environment (e.g. ABAQUS) [4]. The code generator stores the domain geometry as a network/graph structure [6], which allows for the admission of a priori unknown element topologies (e.g. particularly important for the automated handling of non-local OBC topologies, see Fig. 4(b)), because the topology's instances are detected using the *symmetry breaking* network motif detection algorithm introduced by Grochow and Kellis [7].

Excerpt from ISBN 978-3-00-053387-7

5. Applications

5.1. Equivalence of MD and MDFEM: Brittle Failure of Carbon Nanotubes with Defects

The MDFEM obtains constitutive fracture responses of CNT with vacancies, Stone-Wales and weakened-bond defects in a highly non-linear environment during both static and dynamic implicit FE analyses [4]. The latter are equivalent to those of a MD study [8], see Fig. 7(a), but are obtained at computationally reduced cost; merely taking $O\left(10^1 - 10^2\right)$ CPU seconds on a standard workstation.

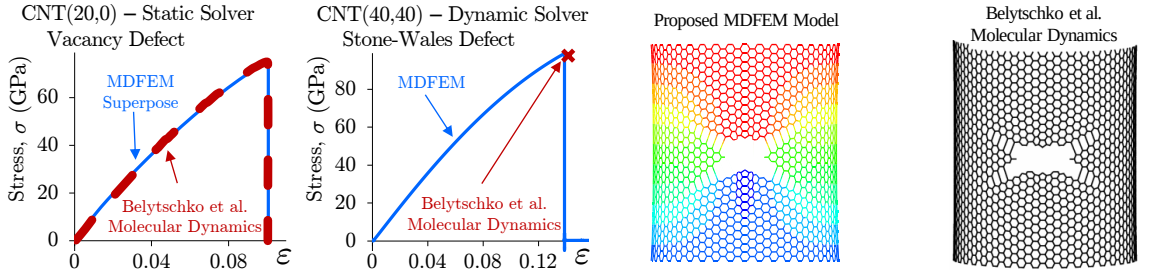

(a) CNT vacancy defect (b) CNT Stone-Wales defect (c) MDFEM failure onset (d) MD failure onset

Figure 6. MDFEM and MD obtain equivalent constitutive frature responses for defective CNT.

5.2. MDFEM Linear computational scaling, eigenvalue analyses & solver strategy flexibility

The implicit static MDFEM exhibits a linear numerical scaling, as shown by axially straining CNT up to 10^6 atoms, i.e $12\,\mu$m long (comparable to experiments), see Fig. 7(a). The implicit dynamic MDFEM solver, unlike an explicit dynamic MD, guarantees converged dynamic equilibrium at highly non-linear points (e.g. fracture onset, see Fig. 6(c)). Moreover, varied solvers are available (e.g. eigenvalue analyses for determining electric-field induced vibrations of molecular devices such as CNT), see Fig. 7(b).

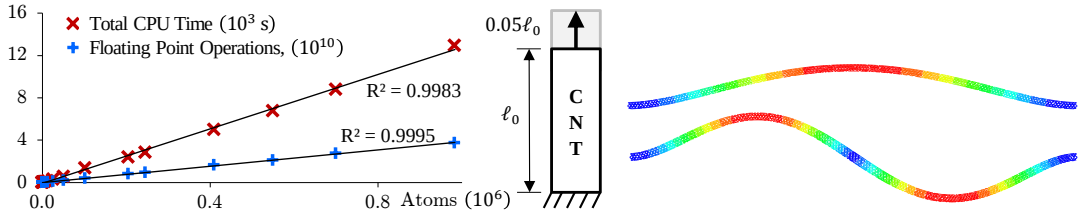

(a) MDFEM exhibits linear computational scaling (b) First modes of CNT frequency analysis

Figure 7. MDFEM has linear scaling and a broad range of solver strategies, e.g. eigenvalue analyses.

5.3. MDFEM Multi-Scale: Hierarchical & Concurrent Integration of MD and FEM Domains

The MDFEM is ideally suited for hierarchical or concurrent multiscale coupling with continuum FEM, see Fig. 8, by avoiding the need for coupling separate numerical solvers and thus allowing for further computational savings. The proposed MDFEM [4] and OBC [5] formulations may be coupled with most existing coupling or hand-shake approaches for smoothing numerical mesh-transitions.

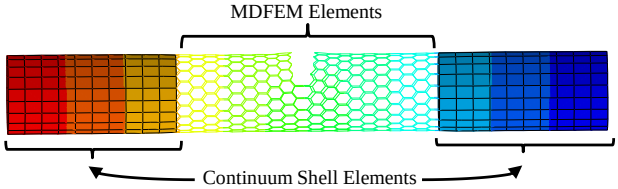

Figure 8. MDFEM achieves further computational savings by concurrently integrating continuum FEM & MD simulations within one solver, such as of this CNT with a discrete defect during fracture.

Excerpt from ISBN 978-3-00-053387-7

5.4. Electro-Mechanical MDFEM: Charge Densities & Electric Field Induced Polarisations

The MDFEM [4], when implemented with advanced anisotropic-polarisation charge-dipole [9], and reactive force fields [10], accurately captures electro-mechanical effects, such as charge induced mechanical strains in CNT, charge distributions in CNT deposited on substrates, pseudo-magnetic fields, electric field induced deflections and vibrations of graphene and CNT. Hence, the virtual design of such electro-mechanical nano-systems within the FEM is rendered possible, see Fig. 9.

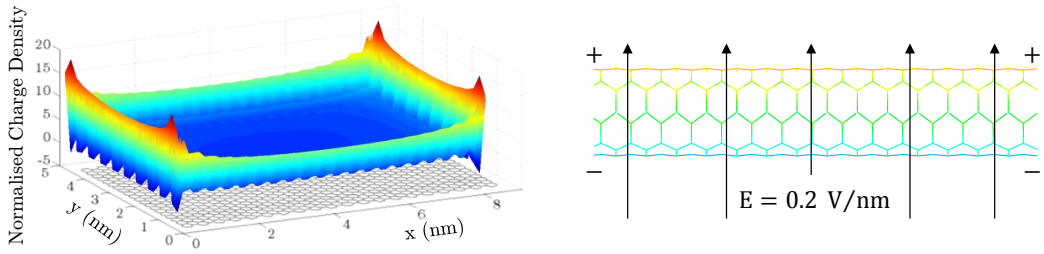

(a) Charged graphene sheet's normalised charge density (b) Electric-field induced polarisation in an insulated CNT

Figure 9. MDFEM is ideally suited to design electro-mechanical devices towards target specifications.

5.5. MDFEM & OBC Property Homogenisation: Graphene and 3D Pillared Graphene Structures

Using MDFEM and both 1st and 2nd order OBC, the properties of graphene and a Pillared Graphene Structure (PGS) were homogenised based on a SD with a *Kinematic Behaviour* consistent with classical Kirchoff plate theory. Hence, the *kinematic parameters* correspond to the plate strains, i.e. in-plane strains/shear/bending/twist, and the homogenised properties are reported as the typical **A** [TPa-nm] and **D** [TPa-nm^3] matrices, see table 1, as to avoid ambiguities with the thickness and continuum assumptions.

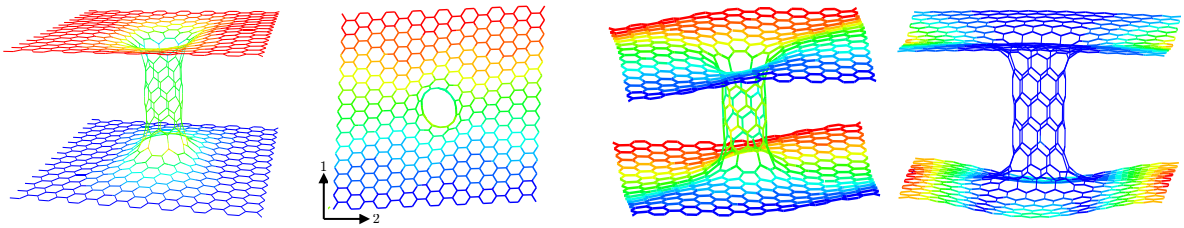

(a) PGS unit cell (b) Top view of pure shear (c) Side view of pure shear (d) Side view of bending

Figure 10. MDFEM can parametrically design novel material nano-structures towards target properties, such as this undeformed PGS unit cell shown in pure shear (top/side-view) and bending.

Table 1. Homogenised Mechanical In-Plane & Bending Properties of Graphene and PGS

	A_{11}	A_{12}	A_{22}	A_{33}	D_{11}	D_{12}	D_{22}	D_{33}
G	0.2242	0.0182	0.2242	0.4044	0.1294×10^{-3}	-	0.1294×10^{-3}	N/A
PGS	0.3392	0.0731	0.3905	0.6409	0.0618	0.1654	0.0735	0.0680

While the PGS's and graphene's in-plane stiffness (**A**) is of the same order of magnitude, the bending properties (**D**) of the PGS are more than two orders of magnitude higher than those of graphene. No twist rigidity is presented for graphene as the used force field does is not applicable for linear twist. Fig. 10 shows that during pure shear as well as bending, the initial small in-plane waviness of the PGS is amplified. Lithium-doped PGS are predicted to possess unrivalled H_2 storage capacities at ambient conditions [11]. Hence, the MDFEM [4] and OBC [5], with their ability to incorporate both advanced mechanical and polarisable charge-dipole force fields, are ideally suited to perform parametric topology studies of the homogenised electro-mechanical, fracture and H_2 storage properties of such hybrid PGS.

Excerpt from ISBN 978-3-00-053387-7

5.6. MDFEM Macro-Scale Simulations: Stress Intensity Factor & Toughness of Graphene

The MDFEM numerical scaling allows for domains beyond 1-2 million atoms, corresponding to macro-sized experimental flake sizes of 0.2-0.5 μm. The stress intensity factors and fracture toughness of graphene was obtained using (i) a macro-sized MDFEM simulation of a pre-cracked graphene together with a crack compliance approach, see Fig. 11(a); (ii) a continuum shell model, based on homogenised properties, where the toughness is obtained through a J-integral approach around the crack opening, see Fig. 11(b); (iii) an analytical model based on chemical bond dissociation energy of sp^2 C-C, see Fig. 11(c). The obtained toughness, in unambiguous energy per unit length dimensions, are consistent across all three approaches, see table 2, although these remain at half of recent experimental results; this is likely due to the experimental measurements being on double-layered multi-grain graphene.

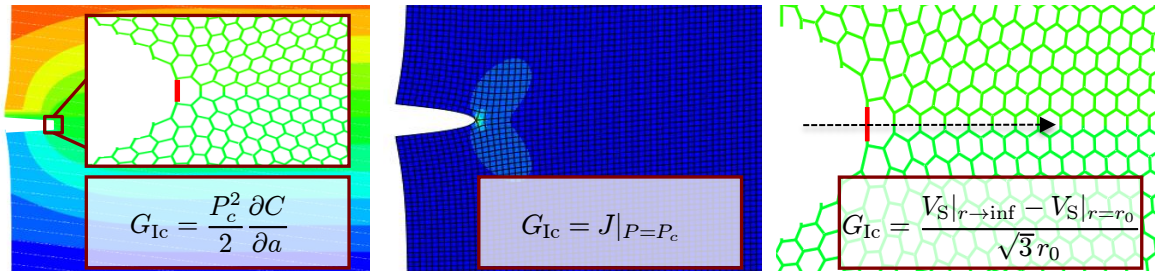

(a) MDFEM macro-simulation (b) Continuum shell model (c) Analytical model

Figure 11. MDFEM can obtain large-scale properties such as toughness through macro-simulations.

Table 2. Graphene Toughness from MDFEM, Continuum, and Analytical Modelling are consistent.

	MDFEM Crack Opening	Continuum Shell J-Integral	Analytical Model	Experimental Measurements [12]
2D G_{Ic} (nJ/m)	2.42	2.69	2.50	5.41

5.7. MDFEM Device Design: Porous Graphene Membrane for DNA Sensor or Desalination

Fig. 12 shows a graphene device where atoms (e.g. potassium, calcium) pass through a pore in the membrane. This is representative for single-molecule DNA sequencing (where the DNA-bases are identified from the membrane's charge response) or for a desalination application. The electro-mechanical response, including the long-range charge/dipole interactions between the thermally oscillating membrane and the non-carbon atoms, is accurately captured and resolved using an implicit dynamic MDFEM. The latter's most distinctive features relative to MD include: (i) guaranteed converged dynamic equilibrium solutions; (ii) stabler time stepping than in an explicit integration procedure; (iii) the ability to have singular mass matrices and thus concurrently solve designs with mechanical displacement as well as multi-physics no-inertia charge/dipole displacements (this requires a two-step MD solver approach).

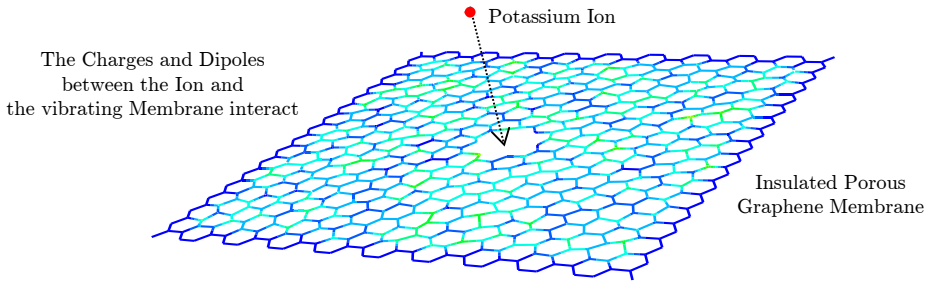

Figure 12. MDFEM can design electro-mechanical devices with good computational flexibility.

Excerpt from ISBN 978-3-00-053387-7

6. Discussion & Conclusion

A *Molecular Dynamics Finite Element Method* (MDFEM) has been presented, together with novel boundary conditions, the *Objective Boundary Conditions* (OBC); representing new contributions to the state of the art in the form of: (i) a mathematically robust multi-physics and multi-scale MDFEM derivation; (ii) a formal separation of force field and element topology information; (iii) a mathematically and numerically optimised implementation; (iv) a symbolic processor based implementation for a fast and high-level MDFEM and OBC implementation; (v) both explicit and implicit FEM formulations, where the latter allows for large time and spacial scales, eigenvalue analyses, and a singular mass matrix; (vi) novel mechanical and charge-dipole FEM results; (vii) the new OBC, which implement local and non-local interactions in low-dimensional structures under under generic torsion/bending deformations; (viii) the ability for readily and implicitly obtaining equivalent homogenised properties of discrete structures; (ix) the ability to admit a priori unknown element topologies for automated mesh generation.

The proposed model represents a unified formulation of MD bridging from small to large time and spacial scales, as well as across different physics, while inherently offering convenient multi-scale and homogenisation integration with continuum FEM. This constitutes a contribution to the pursued ***integrated virtual engineering design and simulation environment***. It will allow for the optimised virtual design of a wide range of electro-mechanical nano-devices and structures to either given device property or macroscopic target specifications (e.g. piezoelectric property couplings in CNT, H_2 storage in PGS), and homogenised properties for different homo- and heteroatomic nano-structures to be used in industrial applications (e.g. structural composites, DNA sensors, flexible electronics).

Acknowledgments

The present project is supported by the National Research Fund, Luxembourg, Grant No.: 1360982.

References

[1] S. Bae, H. Kim, Y. Lee, X. Xu, J.S. Park, Y. Zheng, J. Balakrishnan, T. Lei, H. Ri Kim, Y. I. Song, Y.J. Kim, Kwang S. Kim, B. Ozyilmaz, J.H. Ahn, B. H. Hong, and S. Iijima. Roll-to-roll production of 30-inch graphene films for transparent electrodes. *Nature Nanotechnology*, 5:574–578, 2010.

[2] Stephen Y Chou, Peter R Krauss, and Preston J Renstrom. Nanoimprint lithography. *Journal of Vacuum Science & Technology B*, 14(6):4129–4133, 1996.

[3] H. Gao, H. Tan, W. Zhang, K. Morton, , and S.Y. Chou. Air cushion press for excellent uniformity, high yield, and fast nanoimprint across a 100 mm field. *Nano Letters*, 6(11):2438–2441, 2006.

[4] A.A.R. Wilmes and S.T. Pinho. A coupled mechanical-charge/dipole molecular dynamics finite element method, with multi-scale applications to the design of graphene nano-devices. *International Journal for Numerical Methods in Engineering*, 100(4):243–276, 2014.

[5] A.A.R. Wilmes and S.T. Pinho. Objective boundary conditions for rotations and/or far-field physical interactions in low-dimensional continuum- or nano-structures and their modular property homogenisation across scales, dimensions and structural theories. Submitted 2016.

[6] A.A.R. Wilmes and S.T. Pinho. On network representations of meshed fem domains and network motif detection for meshing spatially non-local as well as a-priori unknown element topologies. Submitted 2016.

[7] J.A. Grochow and M. Kellis. Network motif discovery using subgraph enumeration and symmetry-breaking. In *Research in Computational Molecular Biology*, pages 92–106. Springer, 2007.

[8] T. Belytschko, S.P. Xiao, G.C. Schatz, and R.S. Ruoff. Atomistic simulations of nanotube fracture. *Phys.Rev.B*, 65:235430, 2002.

[9] A. Mayer. Formulation in terms of normalized propagators of a charge-dipole model enabling the calculation of the polarization properties of fullerenes and carbon nanotubes. *Phys.Rev.B*, 75:045407, 2007.

[10] S.J. Stuart, A.B. Tutein, and J.A. Harrison. A reactive potential for hydrocarbons with intermolecular interactions. *J.Chem.Phys.*, 112:6472–6486, 2000.

[11] G.K. Dimitrakakis, E. Tylianakis, and G.E. Froudakis. Pillared graphene: A new 3-d network nanostructure for enhanced hydrogen storage. *Nano Letters*, 8:3166–3170, 2008.

[12] F. Fan Z. Zeng C. Peng P.E. Loya Z. Liu Y. Gong J. Zhang X. Zhang P.M. Ajayan T. Zhu P. Zhang, L. Ma and J. Lou. Fracture toughness of graphene. *Nature Communications*, 2014.

Excerpt from ISBN 978-3-00-053387-7